OF GENES AND MACHINES: APPLICATION OF A COMBINATION OF MACHINE LEARNING TOOLS TO ASTRONOMY DATA SETS

S. Heinis[1], S. Kumar[1], S. Gezari[1], W. S. Burgett[2], K. C. Chambers[2], P. W. Draper[3], H. Flewelling[2], N. Kaiser[2], E. A. Magnier[2], N. Metcalfe[3], AND C. Waters[2]

[1] Department of Astronomy, University of Maryland, College Park, MD, USA
[2] Institute for Astronomy, University of Hawaii at Manoa, Honolulu, HI 96822, USA
[3] Department of Physics, Durham University, South Road, Durham DH1 3LE, UK

ABSTRACT

We apply a combination of genetic algorithm (GA) and support vector machine (SVM) machine learning algorithms to solve two important problems faced by the astronomical community: star–galaxy separation and photometric redshift estimation of galaxies in survey catalogs. We use the GA to select the relevant features in the first step, followed by optimization of SVM parameters in the second step to obtain an optimal set of parameters to classify or regress, in the process of which we avoid overfitting. We apply our method to star–galaxy separation in Pan-STARRS1 data. We show that our method correctly classifies 98% of objects down to $i_{P1} = 24.5$, with a completeness (or true positive rate) of 99% for galaxies and 88% for stars. By combining colors with morphology, our star–galaxy separation method yields better results than the new SExtractor classifier `spread_model`, in particular at the faint end ($i_{P1} > 22$). We also use our method to derive photometric redshifts for galaxies in the COSMOS bright multiwavelength data set down to an error in $(1 + z)$ of $\sigma = 0.013$, which compares well with estimates from spectral energy distribution fitting on the same data ($\sigma = 0.007$) while making a significantly smaller number of assumptions.

Key words: methods: numerical

1. INTRODUCTION

Astronomy has witnessed an ever-increasing deluge of data over the past decade. Future surveys will gather very large amounts of data daily that will require on-the-fly analysis to limit the amount of data that can be stored or analyzed and to allow timely discoveries of candidates to be followed up: examples are Euclid (Laureijs et al. 2011, 100 GB per day), WFIRST (Spergel et al. 2015, 1.3 TB per day), and the Large Synoptic Survey Telescope (Ivezic et al. 2008, 10 TB per day). The evolution of the type, volume, and cadence of the astronomical data requires the advent of robust methods that will enable a maximal rate of extraction of information from the data. Thus, for a given problem, one needs to make sure all the relevant information is made available in the first step, followed by the use of a suitable method that is able to narrow down the important aspects of the data. This can be done both for feature selection and for noise filtering.

In machine learning parlance, the tasks required can be designated as classification tasks (derive a discrete value: star versus galaxy, for instance) or regression tasks (derive a continuous value: photometric redshift, for instance.) Methods for classification or regression usually are of two kinds: physically motivated or empirical.[4] Physically motivated methods use templates built from previously observed data, like star or galaxy spectral energy distributions (SEDs), for instance, in the case of determining photometric redshifts. They also attempt to include as much knowledge as we have of the processes involved in the problem at stake, such as prior information. Physically motivated methods seem more appropriate than empirical, but the very fact that they require a good knowledge of the physics involved might be an important

limitation. Indeed, our knowledge of a number of the processes involved in shaping the SEDs of galaxies, for instance, is still quite limited (e.g., Conroy et al. 2010, and references therein), whether it is about the processes driving star formation, dust attenuation laws, initial mass function, star formation history, or active galactic nucleus (AGN) contribution. Hence, choices need to be made: either make a number of assumptions, in order to reduce the number of free parameters, or decide to be more inclusive and add more parameters, but at the cost of potential degeneracies. Physically motivated methods are also usually limited in the way they treat the correlation between the properties of the objects because the only correlations taken into account are those included in the models used and might not reflect all of the information contained in the data.

On the other hand, empirical methods require few or no assumptions about the physics of the problem. The goal of an empirical method is to build a decision function from the data themselves. The quality of the generalization of the results to a full data set depends of course on the representativeness of the training sample. We note, however, that the question of the generalization also applies to physically motivated methods because they are also validated on the training data.

Depending on the methods used, transformations may need to be effected before the method is applied; for example, in the case of support vector machines (SVM; e.g., Boser et al. 1992; Cortes & Vapnik 1995; Vapnik 1995, 1998; Smola & Schölkopf 1998; Duda et al. 2001), linear separability is presumed, thereby requiring nonlinearly separable or regressible data to be kernel transformed to enable this.

A challenge with empirical methods is that with growing numbers of input parameters, it becomes prohibitive in terms of CPU time to use all of them. It can also be counterproductive to feed the machine learning tool with all of these parameters because some of them might either be too noisy or not bring

---

[4] Formalisms that blend physically motivated and empirical methods have been proposed; see, e.g., Budavári (2009).

any relevant information to the specific problem being tackled. Moreover, high-dimensional problems suffer from being overfit by machine learning methods (Cawley & Talbot 2010), thereby yielding high-dimensional nonoptimal solutions. This requires subselection of relevant variables from a large N-dimensional space (with N potentially close to 1000). This task itself can also be achieved using machine learning tools. Here we present, to our knowledge, the first application to astronomy of the combination of two machine learning techniques: genetic algorithms (GA; e.g., Steeb 2014) for selecting relevant features, followed by SVMs to build a decision–reward function. GAs alone have already been used in astronomy, for instance, in the study of orbits of exoplanets and the SEDs of young stellar objects (Cantó et al. 2009), the analysis of SN Ia data (Nesseris 2011), the study of star-formation and metal-enrichment histories of a resolved stellar system (Small et al. 2013), the detection of globular clusters from *Hubble Space Telescope* (*HST*) imaging (Cavuoti et al. 2014), and photometric redshift estimation (Hogan et al. 2015). At the same time, SVMs have been extensively used to solve a number of problems, such as object classification (Zhang & Zhao 2004), the identification of red variable sources (Woźniak et al. 2004), photometric redshift estimation (Wadadekar 2005), morphological classification (Huertas-Company et al. 2011), and parameter estimation for *Gaia* spectrophotometry (Liu et al. 2012). We note also that the combination of GA and SVM has already been used in a number of fields, such as cancer classification (e.g., Huerta et al. 2006; Albda et al. 2007), chemistry (e.g., Fatemi & Gharaghani 2007), and bankruptcy prediction (e.g., Min et al. 2006). We do not attempt here to provide the most optimized results from this combination of methods. Rather, we present a proof of concept that shows that GA and SVM yield remarkable results when combined, as opposed to using the SVM as a standalone tool.

In this paper, we focus on two tasks frequently seen in large surveys: star–galaxy separation and the determination of photometric redshifts of distant galaxies. Star–galaxy separation is a classification problem that has usually been constrained purely from the morphology of the objects (e.g., Kron 1980; Bertin & Arnouts 1996; Stoughton et al. 2002). A number of studies have used color information with template fitting to separate stars from galaxies (e.g., Fadely et al. 2012). On top of these two common approaches, good results have been obtained by feeding morphology and colors to machine learning techniques (e.g., Vasconcellos et al. 2011; Saglia et al. 2012; Kovács & Szapudi 2015). Our goal here is to extend the star–galaxy separation to faint magnitudes, where the morphology is not as reliable. We apply here the combination of GA with SVM to star–galaxy separation in the Pan-STARRS1 (PS1) Medium Deep Survey (Kaiser et al. 2010; Tonry et al. 2012; Rest et al. 2014).

On the other hand, the determination of photometric redshifts is a well-studied problem of regression that has been dealt with using a variety of methods, including template fitting (e.g., Arnouts et al. 1999; Benítez 2000; Brammer et al. 2008; Ilbert et al. 2009), cross-correlation functions (Rahman et al. 2015), random forests (Carliles et al. 2010), neural networks (Collister et al. 2007), polynomial fitting (Connolly et al. 1995), and symbolic regression (Krone-Martins et al. 2014). We apply the GA-SVM to the zCOSMOS bright sample (Lilly et al. 2007).

The outline of this paper is as follows. In Section 2 we present the data to which we apply our methods and the training sets we use: PS1 and zCOSMOS bright. In Section 3 we briefly describe our methods; we include a more detailed description of SVM in an Appendix. We present our results in Section 4 and finally list our conclusions.

2. DATA

We perform star–galaxy separation in PS1 Medium Deep data (Section 2.1), using a training set built from COSMOS Advanced Camera for Surveys (ACS) imaging (Section 2.2.1). We then derive photometric redshifts for the zCOSMOS bright sample (Section 2.2.2).

2.1. Pan-STARRS1 Data

The Pan-STARRS1 survey (Kaiser et al. 2010) surveyed three-quarters of the northern hemisphere ($\delta > -30°$) in five filters: g_{P1}, r_{P1}, i_{P1}, z_{P1}, and y_{P1} (Tonry et al. 2012). In addition, PS1 has obtained deeper imaging in 10 fields (amounting to 80 deg^2) called the Medium Deep Survey (Tonry et al. 2012; Rest et al. 2014). We use here data in the MD04 field, which overlap the COSMOS survey (Scoville et al. 2007).

We use our own reduction of the PS1 data in the Medium Deep Survey. We use the image stacks generated by the Image Processing Pipeline (Magnier 2006) and also the CFHT u-band data obtained by E. Magnier as follow-up of the Medium Deep fields. We have at hand six bands: u_{CFHT}, g_{P1}, r_{P1}, i_{P1}, z_{P1}, and y_{P1}. We perform photometry using the following steps, considering PS1 *skycell* as the smallest entity: (1) resample (using `SWarp`, Bertin et al. 2002) the u-band images to the PS1 resolution, and register all images; (2) for each band, fit the point-spread function (PSF) to a Moffat function and match that PSF to the worst PSF in each skycell; (3) using these PSF-matched images, we derive a χ^2 image (Szalay et al. 1999); (4) we perform photometry using the `SExtractor` dual mode (Bertin & Arnouts 1996), detecting objects in the χ^2 image and measuring the fluxes in the PSF-matched images: the Kron-like apertures are defined from the χ^2 image and hence are the same over all bands; (5) for each detection, we measure `spread_model` in each band on the original, non-PSF-matched images. We consider here Kron magnitudes, which are designed to contain ~90% of the source light, regardless of being from a point-source star or an extended galaxy.

Here, `spread_model` (Soumagnac et al. 2013) is a discriminant between the local PSF, measured with `PSFEx` (Bertin 2011), and a circular exponential model of scale length FWHM/16 convolved with that PSF. This discriminant has been shown to perform better than SExtractor's previous morphological classifier, `class_star`.

2.2. COSMOS Data

2.2.1. Star–Galaxy Classification Training Set

We use the star–galaxy classification from Leauthaud et al. (2007) derived from high-spatial-resolution *HST* imaging (in the $F814W$ band) as our training set for star–galaxy classification. They separate stars from galaxies based on their `SExtractor` `mag_auto` and `mu_max` (peak surface brightness above surface level). By comparing the derived stellar counts with the models of Robin et al. (2007), Leauthaud et al. (2007) showed that the stellar counts are in excellent agreement

with the models for $20 < F814W < 25$. We perform here star–galaxy separation down to $i_{P1} = 24.5$.

2.2.2. Spectroscopic Redshift Training Set

We use data taken as part of the COSMOS survey (Scoville et al. 2007). We focus here on objects with spectroscopic redshifts obtained during the zCOSMOS bright campaign (Lilly et al. 2007, $i < 22.5$). We use the photometry obtained in 25 bands by various groups in broad optical and near-infrared bands (Capak et al. (2007, u^*, B_J, V_J, g^+, r^+, i^+, z^+, K_s), in narrow bands (Taniguchi et al. 2007, NB816; Ilbert et al. 2009, NB711), and in intermediate bands (Ilbert et al. 2009, IA427, IA464, IA505, IA574, IA709, IA827, IA484, IA527, IA624, IA679, IA738, IA767). We also use IRAC1 and IRAC2 photometry (Sanders et al. 2007). We consider here only objects with good redshift determination (confidence class: 3.5 and 4.5), $z < 1.5$ (which yields 5807 objects) and measured magnitudes for all the bands listed above, which finally leaves us with 5093 objects. We do not use objects with other confidence-class values because the spectroscopic redshifts can be erroneous in at least 15% of cases (O. Ilbert 2016, private communication).

3. METHODS

We present here the two machine learning methods we use in this work: GAs are used to select the relevant features, and SVMs are used to predict the property of interest using these features.

3.1. Genetic Algorithms

GAs (e.g., Steeb 2014) apply the basic premise of genetics to the evolution of solution sets of a problem until they reach optimality. The definition of optimality itself is debatable, but the general idea is to use a reward function to direct the evolution. That is, we evolve solution sets of parameters (or genes) known as organisms through several generations according to some predefined evolutionary reward function. The reward function may be a goodness of fit or a function thereof that may take into account more than just the goodness of fit. For example, one may choose to determine subsets of parameters that optimize χ^2 or likelihood, Akaike information criteria, energy functions, or entropy. The lengths of the first generation of organisms are chosen to range from the minimum expected dimensionality of the parameter space (which can be one) to the maximum expected dimensionality of the covariance.

The fittest organisms in a particular generation are then given higher probabilities of being chosen to be the parents for successive generations using a roulette selection method based on their fitnesses. Parents are then crossbred using a customized procedure; in our method we first choose the lengths of the children to be based on a tapered distribution where the taper depends on the fitnesses of the parents. That way the length of the child is closer to that of the fitter parent. The child is then populated using the genes of both parents, where genes that are present in both parents are given twice the weight of genes that are only present in one parent. The idea is that the child should, with a greater probability, contain genes that are present in both parents, as opposed to the ones contained in only one of them. This process iteratively produces fitter children in successive generations and is

terminated when no further improvement in the average organism quality is seen. Like in biological genetics, we also introduce a mutation in the genes with constant probability. The genes that are chosen to be mutated are replaced with any of the genes that are not part of either parent, with a uniform probability of choosing from the remaining genes. This allows for genes that are not part of the current gene pool to be expressed. The conceptual simplicity of GA combined with their evolutionary analogy as applied to some of the hardest multiparameter global optimization problems makes them highly sought after.

3.2. Support Vector Machines

SVM (e.g., Boser et al. 1992; Cortes & Vapnik 1995; Vapnik 1995, 1998; Smola & Schölkopf 1998; Duda et al. 2001) is a machine learning algorithm that constructs a maximum-margin hyperplane to separate linearly separable patterns. SVM is especially efficient in high-dimensional parameter spaces, where separating two classes of objects is a hard problem, and performs with best-case complexity $\mathcal{O}n_{\mathrm{parameters}}n_{\mathrm{samples}}^2$. Where the data are not linearly separable, a kernel transformation can be applied to map the original parameter space to a higher-dimension feature space where the data become linearly separable. For both problems we attempt to solve in this paper, we use a Gaussian radial basis function kernel, defined as

$$K(x, x') = \exp(-\gamma \|x - x'\|^2). \qquad (1)$$

Another advantage of using SVM is that there are established guarantees of their performance, which have been well documented in the literature. Also, the final classification plane is not affected by local minima in the classification or regression statistic, which other methods based on least squares or maximum likelihood may not guarantee. For a detailed description of SVM, please refer to Smola & Schölkopf (1998) and Vapnik (1995, 1998). We use here the Python implementation within the Scikit-learn (Pedregosa et al. 2011) module.

3.3. Optimization Procedure

We combine the GA and SVM to select the optimal set of parameters that enables one to classify objects or derive photometric redshifts. In either case, we first gather all input parameters and then build color combinations from all available magnitudes. We also consider here transformations of the parameters, namely their logarithm and exponential on top of their catalog values, which we name "linear" afterward, in order to capture nonlinear dependencies on the parameters. Note that any transformation could be used; we limited ourselves to log and exp for the sake of simplicity for this first application. This way, the rate of change of the dependent parameter as a function of the independent parameter in question is more accurately captured, and dependencies on multiple transformations of the same variable can also be captured. To eliminate scaling issues in transformed spaces, we transform all independent parameters to between -1 and 1. The optimization is then performed in the following two steps iteratively until the end criterion or convergence criterion is met: selection of the relevant set of features in the first, and automatic optimization of SVM parameters to yield optimal classification/regression given the parameters. For SVM classification, the true positive rate is used as the fitness
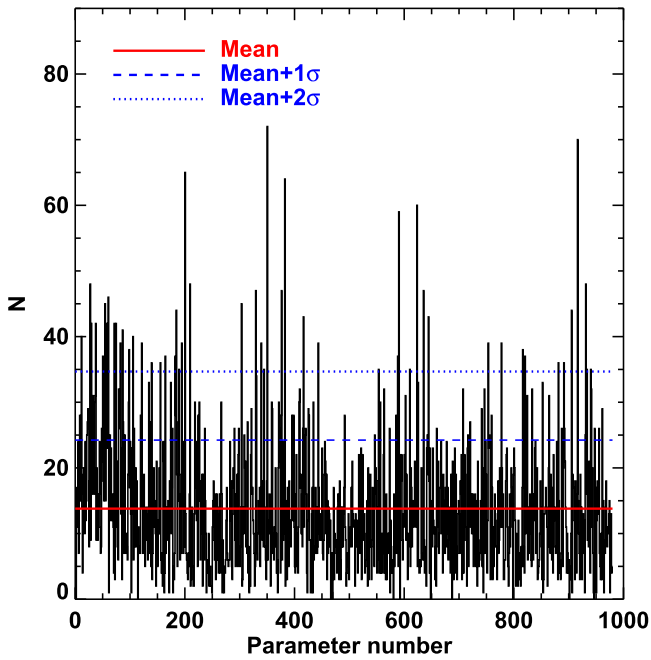
Figure 1. Example of posterior distribution for the parameters obtained from the GA-SVM. This posterior distribution was derived for the application to photometric redshifts (Section 4.2). The red solid line shows the average occurrence of the parameters, the dashed blue line the occurrence at the mean plus one standard deviation, and the dotted blue line the occurrence at the mean plus two standard deviations. We use here all parameters that appear more times than the mean plus one standard deviation in the posterior distribution.

function. For SVM regression, a custom fitness function based on the problem at hand is chosen. For example, for SVM regressions on the photometric redshift we use

$$\frac{1}{\sum_i \left(\frac{z_{\text{phot}}^i - z_{\text{spec}}^i}{z_{\text{phot}}^i}\right)^2}. \qquad (2)$$

Once the fitness of all organisms has been evaluated, a new generation of the same size as the parent generation is created using roulette selection. The GA then runs until it reaches a predefined stopping criterion. We use here the posterior distribution of the parameters. We stop the GA when all parameters have been used at least 10 times. We also use the posterior distribution to choose the optimal set of parameters. Various schemes can be defined. For our application, we restrict ourselves to characterizing the posterior distribution by its mean μ and standard deviation σ (see Figure 1). We consider here all parameters that appear more than $\mu + \sigma$ or $\mu + 2\sigma$ times in the posterior distribution, depending on which of our results change significantly. For instance, in the case of photometric redshifts, the mean of the posterior distribution is $\mu = 13.8$, and the standard deviation is $\sigma = 10.4$; we keep all parameters that occur more than 24 times in the posterior distribution when using the $\mu + \sigma$ criterion.

3.3.1. SVM Parameter Optimization

SVM are not "black boxes" but come with a well-defined formalism and free parameters to be adjusted. For this application, we use the νSVM version of the algorithm, which allows us to control the fractional error and the lower limit on the fraction of support vectors used. We use here $\nu = 0.1$. In the case of classification (star–galaxy separation), we are then

Table 1
Star–Galaxy Separation: GA Output Parameters

Parameter	Transform	Occurrence Threshold[a]
u_{CFHT}	log	$\mu + \sigma$
r_{P1}	lin	$\mu + \sigma$
r_{P1}	log	$\mu + 2\sigma$
`spread_model_g`	exp	$\mu + \sigma$
`spread_model_r`	lin	$\mu + 2\sigma$
`spread_model_r`	log	$\mu + 2\sigma$
`spread_model_i`	exp	$\mu + 2\sigma$
$u_{\text{CFHT}} - g_{\text{P1}}$	lin	$\mu + \sigma$
$u_{\text{CFHT}} - z_{\text{P1}}$	lin	$\mu + \sigma$
$u_{\text{CFHT}} - y_{\text{P1}}$	lin	$\mu + 2\sigma$
$g_{\text{P1}} - y_{\text{P1}}$	log	$\mu + \sigma$
$r_{\text{P1}} - y_{\text{P1}}$	exp	$\mu + \sigma$
$i_{\text{P1}} - y_{\text{P1}}$	lin	$\mu + \sigma$
$z_{\text{P1}} - y_{\text{P1}}$	exp	$\mu + \sigma$
z_{phot}	lin	$\mu + \sigma$

Note.
[a] Here, $\mu + \sigma$ indicates that the parameter occurred at least $\mu + \sigma$ times in the posterior distribution of the GA, while $\mu + 2\sigma$ indicates that the parameter occurred $\mu + 2\sigma$ times.

left with only one free parameter, the inverse of the width of the Gaussian kernel, γ (Equation (1)). In the case of regression (photometric redshifts), we have an additional free parameter, the trade-off parameter C (see Appendix).

If not used with caution, machine learning methods can lead to overfitting: the decision function is biased by the training sample and will not perform well on other samples. In order to avoid overfitting and optimize the values of γ and C, we perform a 10-fold cross-validation, in which we divide the sample into 10 subsets, and we then perform classification or regression for each subset after training on the nine other subsets. We perform this cross-validation for a grid of γ and C values. In the case of SVM, the overfitting can be measured by the fraction of objects used as support vectors, f_{SV}. If $f_{\text{SV}} \sim 1$, most of the training sample is used as support vectors, which will lead to poor generalization. For each iteration, we also get f_{SV}, in order to include it in our cost function. For both applications, we minimize a custom cost function that optimizes the quality of the classification or regression, and f_{SV}.

4. RESULTS

4.1. Star–Galaxy Separation

We use as inputs to the GA feature selection step all magnitudes available for the PS1 data set: u_{CFHT}, g_{P1}, r_{P1}, i_{P1}, z_{P1}, and y_{P1}; the `spread_model` values derived from each of these bands; and the ellipticity measured on the χ^2 image, with all colors. We also included a few quantities determined by running the code `lephare` on these data: the photometric redshift and the ratios of the minimum χ^2 using galaxy, star, and quasar templates: $\chi^2_{\text{galaxy}}/\chi^2_{\text{star}}$, $\chi^2_{\text{galaxy}}/\chi^2_{\text{quasar}}$, and $\chi^2_{\text{quasar}}/\chi^2_{\text{star}}$. Including the transformations of these parameters yields 96 input parameters to the GA-SVM feature selection procedure.

The parameters selected by the GA with occurrence larger than $\mu + \sigma$ times in the posterior distribution are listed in
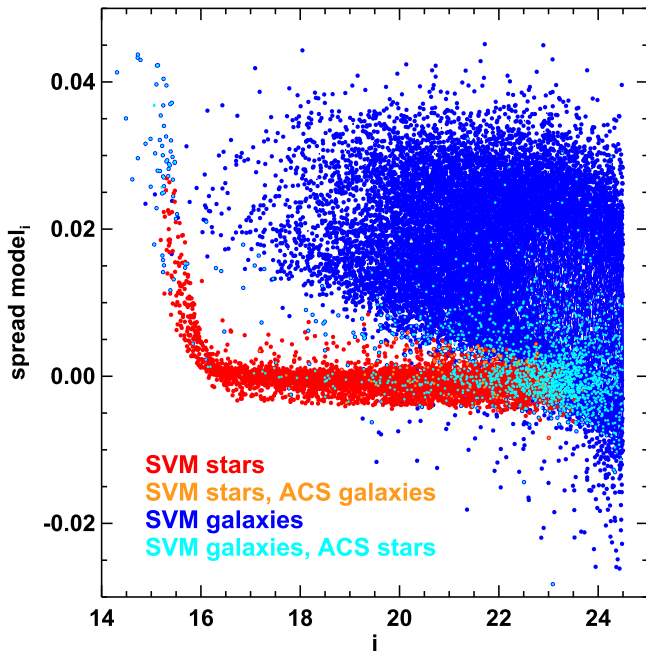
Figure 2. SExtractor morphological classifier `spread_model` measured in the PS1 i band as a function of i_{P1}. We also show the result of our baseline classification (training on all objects): red points show objects classified as stars by the GA-SVM, and blue points show objects classified as galaxies. Orange and cyan points show misclassified objects: orange points are galaxies according to the catalog of Leauthaud et al. (2007) classified as stars, and cyan points are stars classified as galaxies.

Table 1. We also indicate the parameters whose occurrence is larger than $\mu + 2\sigma$ times. The 15 selected parameters include `spread_model` derived in g_{P1}, r_{P1}, and i_{P1}, but are dominated by colors (seven of 15). Using the parameters occurring more than $\mu + 2\sigma$ yields similar results, although with significant overfitting.

In order to quantify the quality of the star–galaxy separation, we use the following definitions for the completeness c and the purity p:

$$c_{\mathrm{g}} = \frac{n_{\mathrm{g}}}{n_{\mathrm{g}} + m_{\mathrm{g}}} \qquad (3)$$

$$p_{\mathrm{g}} = \frac{n_{\mathrm{g}}}{n_{\mathrm{g}} + m_{\mathrm{s}}} \qquad (4)$$

where n_x is the number of objects of class x correctly classified, and m_x is the number of objects of class x misclassified. The same definition holds for the star completeness and purity.

Based on these definitions, in the case of star–galaxy separation, we use this as the cost function:

$$J = \left(\frac{c_{\mathrm{g}} - 1}{0.005}\right)^2 + \left(\frac{c_{\mathrm{s}} - 1}{0.005}\right)^2 + \left(\frac{p_{\mathrm{g}} - 1}{0.005}\right)^2$$
$$+ \left(\frac{p_{\mathrm{s}} - 1}{0.005}\right)^2 + \left(\frac{f_{\mathrm{SV}} - 0.1}{0.01}\right)^2. \qquad (5)$$

In other words, we choose here to optimize the average completeness and purity for stars and galaxies and also penalize high f_{SV}, which amounts to penalizing high fractional errors, and overfitting as well. Other optimization schemes can be adopted. We perform the optimization over the only SVM free parameter here, the inverse of the width of the Gaussian kernel,

Table 2
Star–Galaxy Separation: Performance

Type	GA-SVM all[a]	GA-SVM Bright/Faint[b]	`spread_model`[c]
All types	97.4	98.1	92.7
Galaxies	99.8	99.2	94.5
Stars	74.5	88.5	75.9

Notes. Percentage of correctly classified objects for each method:
[a] Training and prediction on the full sample.
[b] Training and prediction on bright and faint objects separately.
[c] SExtractor `spread_model` method.

γ. We use a grid search using a log-spaced binning for $0.01 < \gamma < 10$.

We show in Figure 2 the `spread_model` derived in the PS1 i band as a function of i_{P1}. Figure 2 shows that `spread_model` enables us to recover a star sequence down to $i_{P1} \sim 22$. At fainter magnitudes, morphology alone is not able to accurately separate stars from galaxies at the PS1 angular resolution. The color coding shows the result of the GA-SVM classification. We classify objects down to $i_{P1} = 24.5$. We choose this limit because the completeness of the PS1 data drops significantly beyond 24.5, and also because the training set we use is valid down to $F814W = 25$. Figure 1 suggests that the GA-SVM is able to recover the classification at bright magnitudes but also to extend it at the faint end. We list in Table 2 the percentage of objects classified correctly. Our method correctly classifies 97% of the objects down to $i_{P1} = 24.5$. We can compare our results to those from the PS1 photometric classification server (Saglia et al. 2012), which used SVM on bright objects using PS1 photometry. They obtained 84.9% of stars correctly classified down to $i_{P1} = 21$ and 97% of galaxies down to $_{P1} = 20$. Our method enables us to improve upon those, as we get 88.6% of stars correctly classified and 99.3% of galaxies correctly classified in the same magnitude range.

We examine in more detail in Figures 3 and 4 the colors of the objects. These figures show that the bulk of stars that are misclassified as galaxies are at the faint end, $i \gtrsim 22$, and that these objects are in regions where the colors of stars and galaxies are similar. Galaxies misclassified as stars are brighter, $i < 22$, but again are in regions where the colors of stars and galaxies overlap. There are also a handful of very bright stars misclassified as galaxies, in a domain where the galaxy sampling is very poor. Finally, we classify as galaxies a few stars showing colors at the outskirts of the color distributions. These objects might be misclassified by the ACS photometry, or the color might be significantly impacted by photometric scatter.

We show in Figure 5 the completeness (left) and purity (right) of our classifications as a function of i_{P1}.

We derive the completeness and purity for each cross-validation subset and show in Figure 5 the average and as error bars the standard deviation. Most of the features of our classification seen in Figure 5 are due to the fact that the training sample is unbalanced at the bright end and the faint end: at the bright end, stars outnumber the galaxies, and the other way around at the faint end. At the bright end ($i_{P1} < 16$, which is also within the saturation regime), the completeness is higher for stars than for galaxies, while noisy because of small statistics. Some bright galaxies are misclassified as stars. At the faint end ($i_{P1} > 22$), the star completeness decreases because
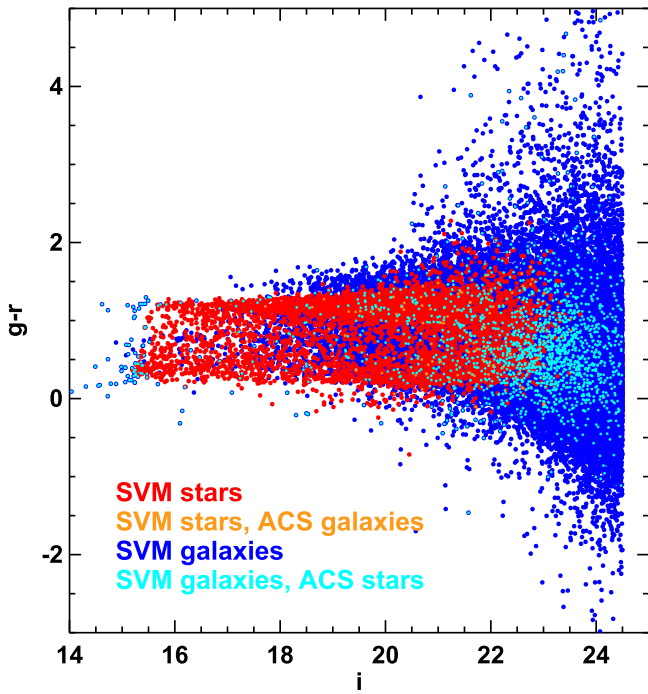
Figure 3. Color–magnitude diagram $g - i_{P1}$ as a function of i_{P1}. The color coding is the same as in Figure 2.

some stars are classified as galaxies. The impression given by Figure 5 is striking, as the star completeness decreases to 0 at $i_{P1} \sim 24$. Note, however, that the stars represent only 3% of the overall population at this flux level (Leauthaud et al. 2007). The purity shows a similar behavior at the bright end. At the faint end, however, the purity of the stars is larger than 0.85 for $i_{P1} \lesssim 23$. For galaxies, both completeness and purity are lower than 0.8 at the bright end ($i_{P1} < 18$), but the number of galaxies is small at these magnitudes. At $i_{P1} > 18$, completeness and purity are independent of magnitude down to $i_{P1} = 24.5$ and larger than 0.95.

We compare these results to the classification obtained with `spread_model` derived in the i_{P1} band. We determine a single cut in `spread_model_i` using its distribution for reference stars and galaxies. Our cut is the value of `spread_model_i` such that $p(\text{g}|\,\texttt{spread\_model\_i}) = p(\text{s}|\,\texttt{spread\_model\_i})$. We show in Figure 5 the completeness and purity obtained with `spread_model_i` as dotted lines. For $i_{P1} \lesssim 22$, the results from `spread_model_i` and our method are similar: at the PS1 resolution, point sources and extended objects are well discriminated in this magnitude range. At $i_{P1} > 22$, our baseline method performs better, in particular for galaxies, which is expected as we add color information. While the galaxies' purity is similar for both methods, the completeness obtained with `spread_model_i` drops to 0.75 at $i_{P1} = 24.5$, but our method yields a completeness consistent with 1 down to this magnitude. For stars, the purity obtained with the two methods is similar. However, the completeness we obtain drops faster than that obtained with `spread_model_i`. In order to see whether we can improve our baseline method, we optimize the SVM parameters independently in two magnitude ranges: $i_{P1} < 22$ and $i_{P1} > 22$. Because galaxies at the faint end outnumber stars by several orders of magnitude, we add an extra free parameter for the optimization at $i_{P1} > 22$, which

attempts to correct this sampling issue. In practice, we use all stars available, but only a fraction of the galaxies available, from one to 10 times the number of stars. The results obtained are shown in solid lines on Figure 5. The results for galaxies are virtually unchanged compared to our baseline method. For stars, we are able to improve at the faint end, where the purity is better than that obtained with `spread_model_i` for $i_{P1} < 23$.

As a final check, we also derive the star–galaxy separation by using SVM only, without selecting the inputs with the GA. The results are only marginally different. We note, however, that a parameter space with lower dimensions is less prone to overfitting with machine learning methods. On the other hand, even with similar results, a SVM-based star–galaxy separation with a smaller number of input parameters is more likely to generalize properly.

4.2. Photometric Redshifts

We used 978 input parameters as inputs for the GA-SVM optimization procedure: all magnitudes and colors available from the COSMOS data set and the transformations of these parameters, as described in Section 3.3. Hereafter we consider the parameters that appear at least $\mu + 1\sigma$ times in the posterior distribution, so we are left with 131 parameters. The parameters retained by the GA-SVM are dominated by colors (82%, 108/131), in particular colors involving intermediate and narrow bands (71%, 93/131). Using the parameters that appear $\mu + 2\sigma$ times in the GA posterior distribution yields 45 parameters, with similar proportions of colors and intermediate and narrow bands. This is in line with the conclusions of studies using SED fitting methods, which show that including narrow and intermediate bands improves significantly the estimation of photometric redshifts (e.g., Ilbert et al. 2009).

We quantify the errors on photometric redshifts as $\text{err}(z_{\text{spec}}) = (z_{\text{phot}} - z_{\text{spec}})/(1 + z_{\text{spec}})$, using as a measure of global accuracy σ, the normalized median absolute deviation, defined as
$\sigma(z) = 1.4826 * \text{median}\,(|\text{err}(z_{\text{spec}}) - \text{median}(\text{err}(z_{\text{spec}}))|)$.

We define the following cost function for the SVM optimization:

$$J = \left(\frac{\sigma(z) - 0.005}{0.0001}\right)^2 + \left(\frac{f_{\text{SV}} - 0.1}{0.01}\right)^2. \qquad (6)$$

We perform the optimization over the two SVM free parameters available here, γ and the trade-off parameter C. We use a grid search using a log-spaced binning for $0.01 < \gamma < 10$ and $0.01 < C < 500$.

We compare in Figure 6 the spectroscopic and photometric redshifts. We obtain an overall accuracy of 0.013.[5] The percentage of outliers, defined as objects with $|\text{err}(z_{\text{spec}})| > 0.15$, is below 1%. The average error (bias) is equivalent to zero; our results do not show any significant bias as a function of redshift. At high redshifts ($z > 1$) the spectroscopic sampling is small, so the model is less constrained. Using the parameters that appear $\mu + 2\sigma$ times in the GA-SVM posterior distribution yields similar results ($\sigma(z) = 0.014$), which shows that by using three times fewer parameters, the same accuracy can be achieved.

---

[5] Using objects with spectroscopic confidence class $3 \leqslant CC < 5$ yields similar results with an accuracy of $\sigma(z) = 0.015$.
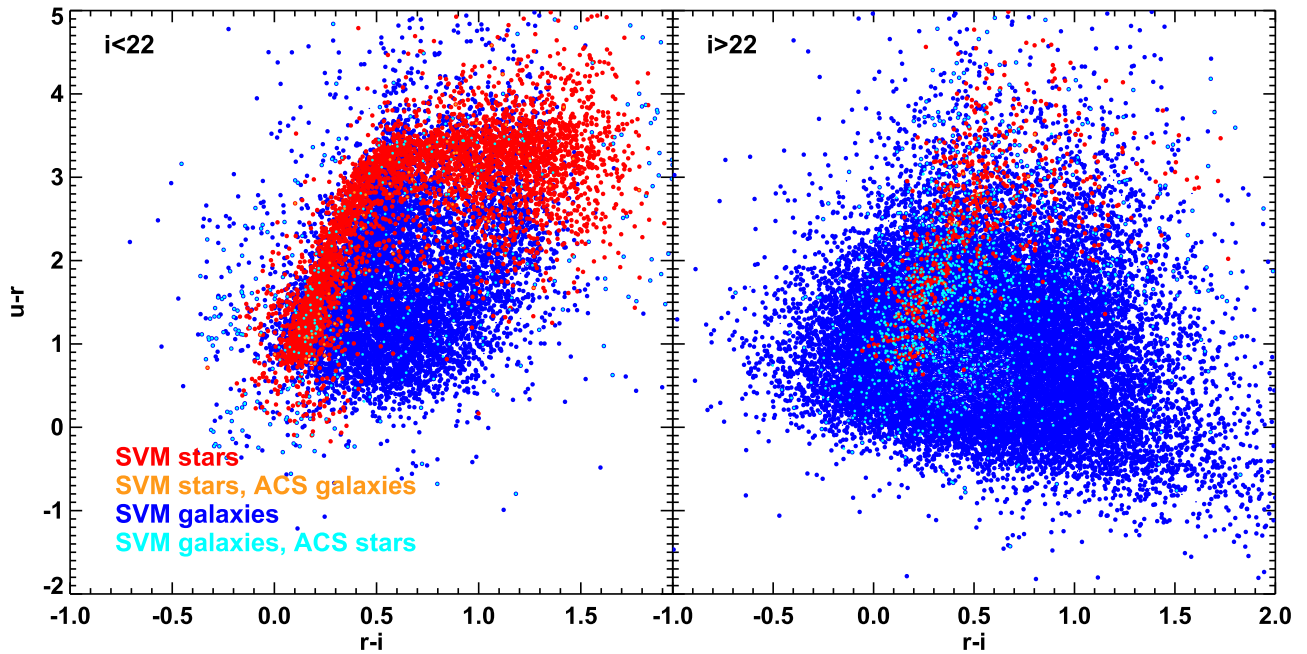
Figure 4. Color–color diagram $u - r_{P1}$ as a function of $r - i_{P1}$. The left panel shows objects with $i_{P1} < 22$ and the right panel objects with $i_{P1} > 22$. The color coding is the same as in Figure 2.

On a similar sample[6], Ilbert et al. (2009), using an SED fitting method, obtained an overall accuracy of 0.007. While our results are slightly worse at face value, we note that we use here only two free parameters for the photometric redshift optimization and one model to derive the photometric redshifts (the one from SVM). In contrast, Ilbert et al. (2009) rely on 21 SED templates, 30 zero-point offsets (one per band), and an extra parameter describing the amount $E(B - V)$ of internal dust attenuation. We also explicitly avoid overfitting, and doing so guarantees the potential for generalization of these results. Our tests show that we can obtain an overall accuracy of ~0.01, but this comes at the price of significant overfitting (the support vectors are made up from the whole sample).

As above, we also derive the photometric redshifts by using SVM only, without selecting the inputs with the GA. In this case the results are much worse, yielding large errors: $\sigma(z) \sim 0.5$. This shows that the combination of GA and SVM yields better results than SVM alone.

We also test whether we can derive empirical error estimates for each object using SVM. We use a variant of the k-fold cross-validation, the so-called "inverse." The usual k-fold cross-validation consists of dividing the sample into k subsamples (we use $k = 10$ here); for each subsample, predictions are made using the SVM trained on the union of the other $k - 1$ subsamples. To derive error estimates, we use the inverse k-fold cross-validation such that we train the SVM on one subsample, and we predict photometric redshifts for the union of the other $k - 1$ subsamples. We have then $k - 1$ estimates of z_{phot}. We derive an empirical error estimate $\hat{\sigma}_z$, which is the standard deviation of these estimates. We show in Figure 7 the normalized distribution of the ratio $(z_{spec} - z_{phot})/\hat{\sigma}_z$. If our empirical estimate were an accurate measurement of the actual error, this distribution should be a normal one. A comparison with a normal distribution shows

that this is indeed the case, which suggests that our error estimates are accurate.

5. CONCLUSIONS

We present a new combination of two machine learning methods that we apply to two common problems in astronomy: star–galaxy separation and photometric redshift estimation. We use GA to select relevant features and SVM to estimate the quantity of interest using the selected features. We show that the combination of these two methods yields remarkable results and offers an interesting opportunity for future large surveys that will gather large amounts of data. In the case of star–galaxy separation, the improvements over existing methods are a consequence of adding more information, while for photometric redshifts, it is rather the selection of the input information fed to the machine learning methods. This shows that the combination of GA and SVM is very efficient in the case of problems with large dimensions.

We first apply the GA-SVM method to star–galaxy separation in the PS1 Medium Deep Survey. Our baseline method correctly classifies 97% of objects, in particular virtually all galaxies. Our results improve upon the new SExtractor morphological classifier, `spread_model`, which is expected because we added color information instead of morphology only. We show how these results can be further improved for stars by training separately bright and faint objects and by taking into account the respective numbers of stars and galaxies to avoid being dominated by one population.

We then apply the GA-SVM method to photometric redshift estimation for the zCOSMOS bright sample. We obtain an accuracy of 0.013, which compares well with the results from SED fitting, as we are using only two free parameters. We also show that we can derive accurate error estimates for the photometric redshifts.

We present here a proof of concept of a new method that can be modified or improved depending on the problem at stake.

---

[6] Ilbert et al. (2009) used an earlier version of the catalog we are using here.
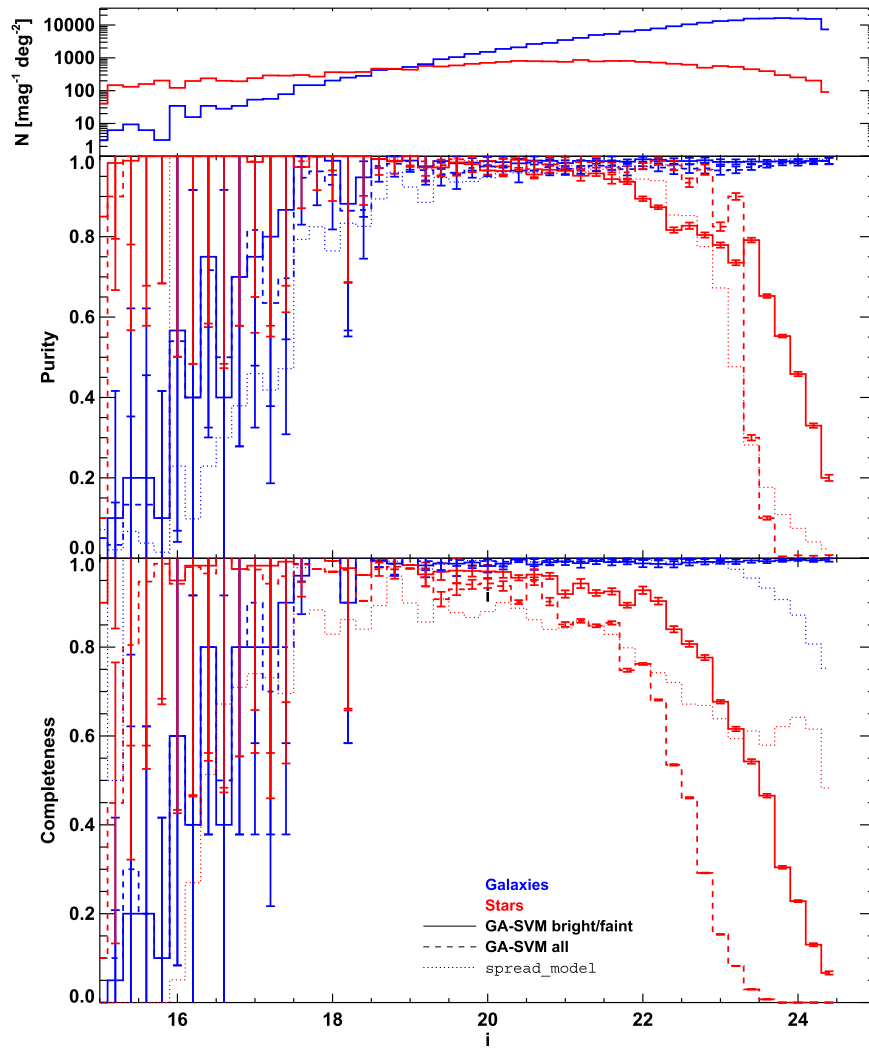
Figure 5. Quality of the GA-SVM star–galaxy classification. Top: galaxy and star counts. Middle: completeness as a function of PS1 i magnitude. Bottom: purity as a function of PS1 i magnitude. On all panels, red is for stars, and blue is for galaxies. On the middle and bottom panels, lines show different classifications: the dashed lines show the result of our classification when training with the full sample; solid lines when training on bright ($i_{P1} > 22$) and faint ($i_{P1} < 22$) objects separately; dotted lines show the classification from spread_model.

For instance, one can substitute another machine learning tool to SVM (such as random forests) to derive the quantity of interest. Furthermore, the criterion used to select the final number of features from the GA posterior distribution can also be optimized beyond the one we use here. All these tools will enable us to use as much information as possible in an efficient way for future large surveys.

APPENDIX
SVM: SHORT DESCRIPTION

We provide here a short description of the SVM. More detailed presentations of the formalism can be found elsewhere (e.g., Vapnik 1995, 1998, Smola & Schölkopf 1998). For the sake of brevity, we present here only the equations relevant to regression with SVM. Equations for classification are similar, except for a few differences that we mention whenever necessary.

The training data usually consists of a number of objects with input parameters, $\boldsymbol{x}$, of any dimension, and the known values of the quantity of interest, $\boldsymbol{y}$. The goal of SVM is to find a function f such that

$$f = \boldsymbol{w} \cdot \boldsymbol{x} + b \qquad (7)$$
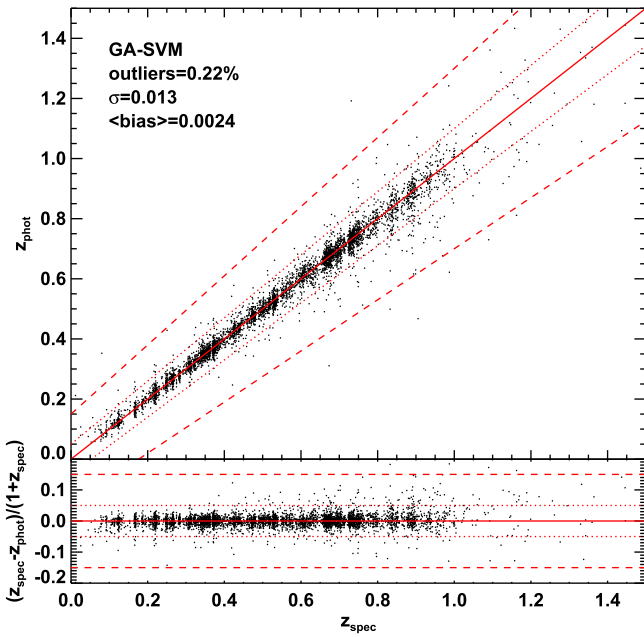
Figure 6. Top: comparison of spectroscopic redshifts with photometric redshifts obtained with the GA-SVM. The solid line shows identity, the dotted line an error of 0.05 in $1 + z$, and the dashed line an error of 0.15 in $1 + z$. Bottom: errors of photometric redshifts as a function of spectroscopic redshifts. Lines are the same as above.
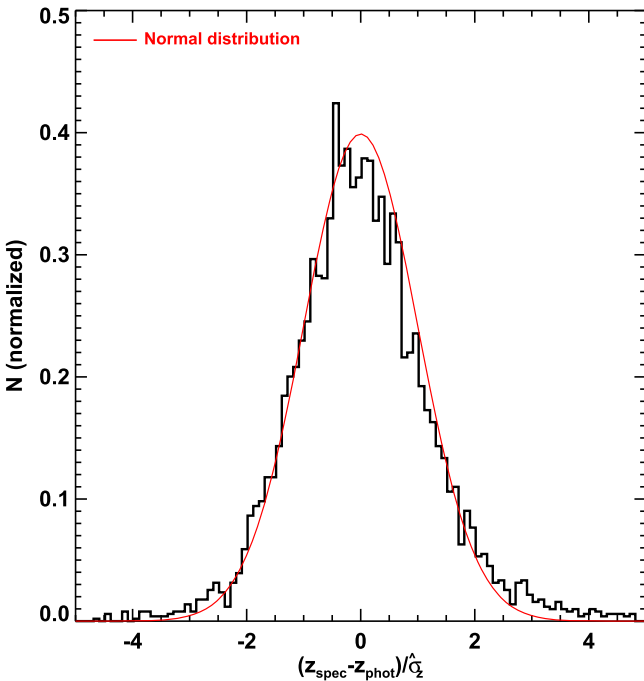
Figure 7. Empirical estimate of photometric redshift errors. The histogram shows the distribution of the ratio $(z_{\rm spec} - z_{\rm phot})/\hat{\sigma}_z$. The curve is a normal distribution.

which yields y with a maximal error ϵ, and like f is as flat as possible. In other words, the amplitude of the slope w has to be minimal. One way to achieve this is to minimize the norm $\frac{1}{2}|w|^2$ with the condition $|y_i - w. x_i - b| \leqslant \epsilon$. The margin in that case is $\frac{2}{|w|}$. In other words, SVM attempts to regress with the largest possible margin.

In a number of problems, the data cannot be separated using a fixed, hard margin. It is then useful to allow some points to be misclassified. One uses a "soft margin," which enables us to allow some errors in the results. The modified minimization reads

$$\text{minimize } \frac{1}{2}|w|^2 + C\sum_i \xi_i + \xi_i^* \qquad (8)$$

$$\text{subject to: } \begin{cases} y_i - w. x_i - b \leqslant \epsilon + \xi_i \\ -y_i + w. x_i + b \leqslant -\epsilon + \xi_i^* \\ \xi_i, \xi_i^* \geqslant 0 \end{cases} \qquad (9)$$

where ξ_i, ξ_i^* are "slack variables," and C is a free parameter that controls the soft margin. The larger the C, the harder is the margin: larger errors are penalized.

Using Lagrange multiplier analysis, it can be shown that the slope w can be written as

$$w = \sum_{i=1}^{n}(\alpha_i - \alpha_i^*)x_i \qquad (10)$$

where α_i, α_i^* are the Lagrange multipliers, which satisfy $\sum_{i=1}^{n}\alpha_i - \alpha_i^* = 0$ and $\alpha_i, \alpha_i^* \in [0, C]$.

Equation (10) shows that the solution of the minimization problem is a linear combination of a number of input data points. In other words, the solution is based on a number of support vectors, the number of training samples where $\alpha_i - \alpha_i^* \neq 0$.

The above equations use the actual values of the data, assuming that the separation can be performed linearly. For most high-dimension problems, this assumption is not valid any more. The fact that only a scalar product between the support vectors and the input data is required enables us to use the so-called "kernel trick." The idea behind the trick is that one can use functions that satisfy a number of conditions to map the input space to another where the separation can be performed linearly. Equation (10) then becomes

$$w = \sum_{i=1}^{n}(\alpha_i - \alpha_i^*)\Phi(x_i) \qquad (11)$$

where the kernel $k(x, x') = \langle \Phi(x)\Phi(x')\rangle$.

Finally, a slightly modified version of the algorithm (νSVR) allows us to determine ϵ and control the number of support vectors. A parameter $\nu \in [0, 1]$ is introduced such that Equation (8) becomes

$$\text{minimize } \frac{1}{2}|w|^2 + C(\nu\epsilon + \sum_i \xi_i + \xi_i^*). \qquad (12)$$

It can be shown that ν is the upper limit on the fraction of errors and the lower limit of the fraction of support vectors.

In the regression case described here, the free parameters for νSVR are the trade-off parameter C and all the kernel parameters (assuming that one fixes ν, which allows control of the error and the fraction of support vectors). In the classification case (νSVC), the free parameters are only those from the kernel which is used because ν replaces the trade-off parameter C, and, again, one would usually fix ν.

REFERENCES

Albda, E., Garcia-Nieto, J., Jourdan, L., & Talbi, E.-G. 2007, in Congress on Evolutionary Computation

Arnouts, S., Cristiani, S., Moscardini, L., et al. 1999, MNRAS, 310, 540
Benítez, N. 2000, ApJ, 536, 571
Bertin, E. 2011, in ASP Conf. Ser. 442, Astronomical Data Analysis Software and Systems XX, ed. D. A. Bohlender, D. Durand, & Thomas H. Handley (San Francisco, CA: ASP), 435
Bertin, E., & Arnouts, S. 1996, A&AS, 117, 393
Bertin, E., Mellier, Y., Radovich, M., et al. 2002, in ASP Conf. Ser. 281, Astronomical Data Analysis Software and Systems XI, ed. I. N. Evans et al., 228
Boser, B. E., Guyon, I. M., & Vapnik, V. N. 1992, in Proc. 5th Annual ACM Workshop on Computational Learning Theory, 144
Brammer, G. B., van Dokkum, P. G., & Coppi, P. 2008, ApJ, 686, 1503
Budavári, T. 2009, ApJ, 695, 747
Cantó, J., Curiel, S., & Martínez-Gómez, E. 2009, A&A, 501, 1259
Capak, P., Aussel, H., Ajiki, M., et al. 2007, ApJS, 172, 99
Carliles, S., Budavári, T., Heinis, S., Priebe, C., & Szalay, A. S. 2010, ApJ, 712, 511
Cavuoti, S., Garofalo, M., Brescia, M., et al. 2014, New A, 26, 12
Cawley, G., & Talbot, N. 2010, Journal of Machine Learning Research, 11, 2079
Collister, A., Lahav, O., Blake, C., et al. 2007, MNRAS, 375, 68
Connolly, A. J., Csabai, I., Szalay, A. S., et al. 1995, AJ, 110, 2655
Conroy, C., White, M., & Gunn, J. E. 2010, ApJ, 708, 58
Cortes, C., & Vapnik, V. N. 1995, Machine Learning, 20, 273
Duda, R. O., Hart, P. E., & Stork, D. G. 2001, Pattern Classification (New York, NY: Wiley)
Fadely, R., Hogg, D. W., & Willman, B. 2012, ApJ, 760, 15
Fatemi, M. H., & Gharaghani, S. 2007, Bioorganic & Medicinal Chemistry, 15, 7746
Hogan, R., Fairbairn, M., & Seeburn, N. 2015, MNRAS, 449, 2040
Huerta, E. B., Duval, B., & Hao, J.-K. 2006, Applications of Evolutionary Computing, 3907, 34
Huertas-Company, M., Aguerri, J. A. L., Bernardi, M., Mei, S., & Sánchez Almeida, J. 2011, A&A, 525, A157
Ilbert, O., Capak, P., Salvato, M., et al. 2009, ApJ, 690, 1236
Ivezic, Z., Tyson, J. A., Abel, B., et al. 2008, arXiv:0805.2366
Kaiser, N., Burgett, W., Chambers, K., et al. 2010, Proc. SPIE, 7733, 77330E
Kovács, A., & Szapudi, I. 2015, MNRAS, 448, 1305
Kron, R. G. 1980, ApJS, 43, 305
Krone-Martins, A., Ishida, E. E. O., & de Souza, R. S. 2014, MNRAS, 443, L34
Laureijs, R., Amiaux, J., Arduini, S., et al. 2011, arXiv:1110.3193
Leauthaud, A., Massey, R., Kneib, J.-P., et al. 2007, ApJS, 172, 219
Lilly, S. J., Le Fèvre, O., Renzini, A., et al. 2007, ApJS, 172, 70
Liu, C., Bailer-Jones, C. A. L., Sordo, R., et al. 2012, MNRAS, 426, 2463
Magnier, E. 2006, in The Advanced Maui Optical and Space Surveillance Technologies Conf. 50, ed. S. Ryan (Maui, HI: The Maui Economic Development Board), E50
Min, S.-H., Lee, J., & Han, I. 2006, Expert Systems with Applications, 31, 652
Nesseris, S. 2011, JPhCS, 283, 012025
Pedregosa, F., Varoquaux, G., Gramfort, A., et al. 2011, Journal of Machine Learning Research, 12, 2825
Rahman, M., Ménard, B., Scranton, R., Schmidt, S. J., & Morrison, C. B. 2015, MNRAS, 447, 3500
Rest, A., Scolnic, D., Foley, R. J., et al. 2014, ApJ, 795, 44
Robin, A. C., Rich, R. M., Aussel, H., et al. 2007, ApJS, 172, 545
Saglia, R. P., Tonry, J. L., Bender, R., et al. 2012, ApJ, 746, 128
Sanders, D. B., Salvato, M., Aussel, H., et al. 2007, ApJS, 172, 86
Scoville, N., Aussel, H., Brusa, M., et al. 2007, ApJS, 172, 1
Small, E. E., Bersier, D., & Salaris, M. 2013, MNRAS, 428, 763
Smola, A. J., & Schölkopf, B. 1998, NeuroCOLT Tech. Rep. NC-TR-98-030
Soumagnac, M. T., Abdalla, F. B., Lahav, O., et al. 2013, arXiv:1306.5236
Spergel, D., Gehrels, N., Baltay, C., et al. 2015, arXiv:1503.03757
Steeb, W. H. 2014, The Nonlinear Workbook (Singapore: World Scientific)
Stoughton, C., Lupton, R. H., Bernardi, M., et al. 2002, AJ, 123, 485
Szalay, A. S., Connolly, A. J., & Szokoly, G. P. 1999, AJ, 117, 68
Taniguchi, Y., Scoville, N., Murayama, T., et al. 2007, ApJS, 172, 9
Tonry, J. L., Stubbs, C. W., Lykke, K. R., et al. 2012, ApJ, 750, 99
Vapnik, V. N. 1995, The Nature of Statistical Learning Theory (Berlin: Springer)
Vapnik, V. N. 1998, Statistical Learning Theory (New York, NY: Wiley)
Vasconcellos, E. C., de Carvalho, R. R., Gal, R. R., et al. 2011, AJ, 141, 189
Wadadekar, Y. 2005, PASP, 117, 79
Woźniak, P. R., Williams, S. J., Vestrand, W. T., & Gupta, V. 2004, AJ, 128, 2965
Zhang, Y., & Zhao, Y. 2004, A&A, 422, 1113